

Phenomenological constraints of the building blocks of the cluster hadronization model

Stefan Gieseke¹, Stefan Kiebacher¹, Simon Plätzer^{2,3}, Jan Friedigkeit²

¹ Institute for Theoretical Physics (ITP), KIT, Wolfgang-Gaede-Straße 1, D-76128 Karlsruhe

² Institute of Physics, NAWI Graz, University of Graz, Universitätsplatz 5, A-8010 Graz, Austria

³ Particle Physics, Faculty of Physics, University of Vienna, Boltzmanngasse 5, A-1090 Wien, Austria

June 12, 2025

Abstract. We introduce building blocks for the cluster hadronization model in light of a new structure, focusing on cluster fission and cluster decay. We propose theoretically motivated matrix elements for cluster fission and decay as building blocks and study some first phenomenological implications at different energies. In particular we develop a set of observables which can be used to dissect the hadronization history and have constraining power on the individual building blocks. Our analysis will be completed by including colour reconnection in a follow-up work.

1 Introduction

The Large Hadron Collider (LHC) has exceeded expectations about the precision at which hadronic observables can be measured at a hadron collider. One key role for the understanding of fully exclusive hadronic final states is attributed to the simulation with Monte Carlo event generators such as *Herwig* [1–4], *Pythia* [5], or *Sherpa* [6]. Phenomenological models enter these simulations to describe the hadronization of the partonic final state and the Multiple Partonic Interactions (MPI). For many observables the uncertainties associated with their modelling are among the largest parts of the systematic errors that are attributed to precision observables. While in the last decades a strong focus in the development of event generators has been the matching and merging of higher order perturbative matrix elements with the parton shower. The parton showers themselves have gained attention only in recent years, with developments demonstrating shower accuracy at higher logarithmic accuracy [7–13], and beyond the limit of leading-colour evolution [14–17]. Hadronization models, however, have received less attention. Only recently it has become clear that parton showers and hadronization can not be viewed in isolation and that they necessarily need to interrelate in light of the requirements of infrared safety and factorized calculations [18].

In this paper we want to address some of the structure of the cluster hadronization model in *Herwig* and point out possible perturbative and non-perturbative input to construct a novel model. We in particular focus on observables which allow to pinpoint a number of deficiencies in the description of the hadronic final state, and the possibility to constrain the building blocks of the model in great detail. While inclusive observables and event shapes from the LEP era have so far been the most important

input to the tuning of hadronization models, we here go beyond and demonstrate that novel observables can allow us to take a deeper look into the structure of the hadronization model, thus complementing the theoretical development behind factorized approaches and evolution equations [18]. There are new data from the Large Hadron Collider (LHC) and from legacy e^+e^- data for detailed phase space distributions of identified particles and their correlations, which show that some of the details in the cluster hadronization model are not adequate for their description. Here we need improvements of the detailed modelling of hadron production from the cluster model.

Our main approach is based on the observation that parton showers and hadronization models cannot be looked at in isolation [18, 19], and that the hadronization model needs to follow a smooth onset from the partonic state generated by the parton shower. Within this approach, the parton shower cutoff is viewed as a factorization scale. It will therefore not strictly serve as a scale below which partons become unresolved or the meaning of partons as quanta of a weakly coupled field becomes meaningless overall. We should rather argue that this scale should at the same time be viewed as an upper bound for the evolution of a hadronization model, using effectively low-scale perturbative processes together with a non-perturbative initial condition, rather than a mere endpoint of the partonic picture. With this idea in mind we will show that further details of the dynamics in the hadronization model can be derived or at least be motivated. Another shortcoming is the close interplay of hadronization and colour-reconnection, which is thus far modelled on a phenomenological basis and not viewed as an integral part of a hadronization model, but for which an equally fundamental motivation exists [18, 20].

In the present work, we focus on the cluster fission and decay dynamics and identify possible perturbative and non-perturbative input to their role in an evolving hadronization model. We will in particular address the roles of phase space and kinematics, as well as the elementary (perturbative) processes which drive the cluster fission process and the final cluster decay to hadrons. We will then also focus on identifying a set of observables which we can use to complement such a design in order to constrain the building blocks and their interplay in the according measurements. A similar analysis for colour reconnection will be presented in a follow-up work, together with a first tuning analysis. In particular, our new model will lead to *less parameters* to be considered in such a tuning, while it introduces more dynamical features. Our work will constitute a key cornerstone to develop and scrutinize a fully evolving hadronization model and to shed light on its infrared cutoff dependence.

The outline of this paper is as follows: In Sec. 2, we present the main framework in which we will analyze and improve the cluster hadronization model. This includes a review of its current state, and the construction of its building blocks in particular towards the kinematic and phase space constraints of the cluster fission and decay processes. In Sec. 3 we study the impact of the modifications onto measured observables, in particular extending the energy range which should be considered to pinpoint low-scale dynamics of the interface between parton showers and hadronization. In Sec. 4 we develop an entire set of observables which can be used to disentangle the various building blocks we propose, and to guide further theoretical development. We then conclude and provide an outlook on the role of colour reconnection, as well as further development of a novel model.

2 Clusters in light of perturbative evolution

Demanding that the hadronization model should smoothly match to the perturbative evolution of the parton shower has been proposed in [18], and in [19], where the cluster fission process, as well as the low-scale splitting of gluons have been viewed as a process which should ultimately been driven by the parton shower dynamics such that a smooth transition can be guaranteed. We will further elaborate on such an approach, and discuss in this section how the cluster model can be generalized and what perturbative building blocks we can identify in its construction, in particular for the cluster fission. We also propose, what non-perturbative dynamics we could assume to govern the cluster decays. Before doing so, we review the structure of the cluster model as it is currently available. This structure will ultimately need to be changed, in particular to respect the infrared safety criterion spelled out in [18] and as such the demand that clusters should include gluons as constituents, however at this point we do not rebuild the entire structure of the cluster model.

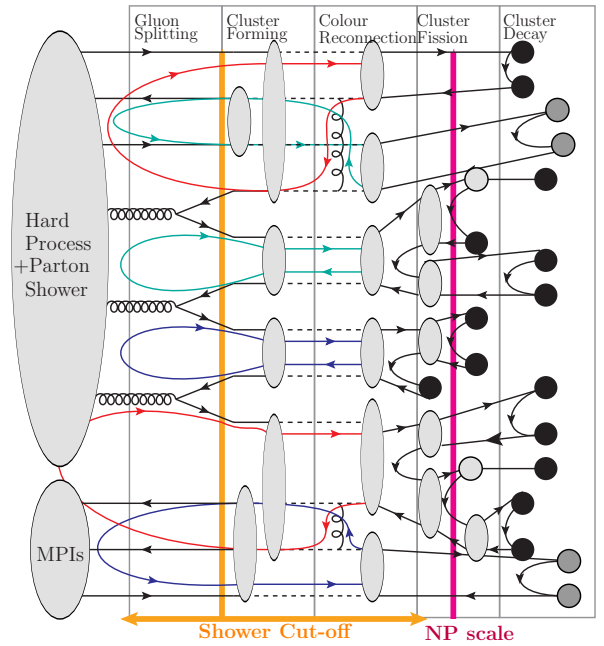
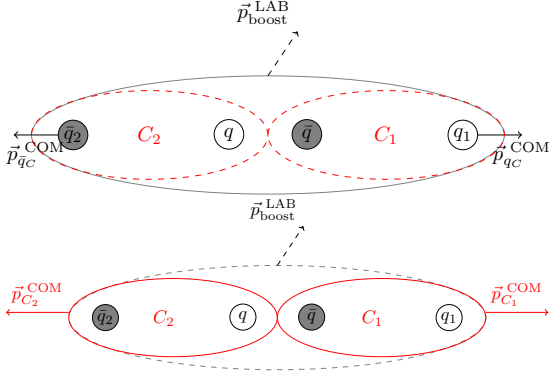


Fig. 1: The structure of the cluster hadronization model. We illustrate how clusters (grey blobs) are formed after the parton shower and the low-scale gluon splitting, how they fission and how they reconnect (*i.e.* how they rescatter), and how they ultimately decay into stable or unstable hadrons (black and dark grey circles). We also indicate some characteristic scales, in particular the parton shower cutoff, and a final, non-perturbative cutoff at which the initial condition of the model is fixed to consist of conversions of clusters into hadrons.

2.1 General structure of the cluster model

In Fig. 1 we show a picture of the hadronization as it evolves from the parton shower. The hadronization generally starts from a partonic final state where all partons are in a certain colour state. Usually the colour state is defined in the limit of large number of colours, N_c , such that all quarks and antiquarks are uniquely assigned to the endpoint of a colour line. Gluons carry both a colour and an anticolour. In order to assign all partons to a colour singlet state in a unique way, all particles, in particular the gluons, are assigned a constituent mass and undergo a number of (small) boosts in order to maintain momentum conservation. This will allow us to decay the gluons non-perturbatively into a light $q\bar{q}$ -pair. The gluon mass is just above the threshold for the creation of this $q\bar{q}$ -pair which implies that even with an isotropic decay the resulting quarks move practically in the original direction of the gluon and share its momentum almost equally and carry the respective colour line of the gluon. As a result, the final state consists of quarks, antiquarks and possibly (anti-)diquarks from the initial hadrons. All particles are in a colour triplet or antitriplet state and rest at the end of a colour line. The colour partner of each particle at the other end of the colour line can be easily found and

Fig. 2: Sketch of current cluster fission model in **Herwig**.

both form one of the so-called primordial clusters. This set of primordial clusters will be the starting point of our studies.

A cluster $C(q_1, q_2)$ is composed of two constituents q_1 and q_2 which generally are one quark or anti-diquark and one anti-quark or diquark and carries the net momentum of these two constituents, resulting in an invariant mass squared $M^2 = (p_1 + p_2)^2$, while the constituents are on their constituent mass-shell. The invariant mass M of the cluster now determines the further steps towards hadronization. Clusters with a large mass M , i.e. M larger than typically 3 – 4 GeV, will fission into pairs of lighter clusters until all clusters are light. We call this process cluster fission. Once all cluster masses are below a certain threshold they will decay into pairs of hadrons, we call this cluster decay. It is possible that a cluster ends up with a mass M that does not leave enough phase space to decay even into the lightest possible pair of hadrons. In this exceptional case, the cluster will decay into a single hadron, while momentum is exchanged with a neighbouring cluster in order to maintain momentum conservation.

The threshold below which clusters decay to hadrons is usually a fixed cutoff, though it has recently been proposed to accompany this parameter by a further smearing. In light of our aim to reduce the number of parameters, while implementing dynamics which follow from a clean theoretical analysis we refrain to use this smearing and interpret the fixed value as the unique point in the evolution when the initial condition has been fixed. In Fig. 2 we sketch a typical cluster fission kinematics. A cluster fission is always carried out when the cluster mass fulfils

$$M \geq [M_{\max}^a + (m_1 + m_2)^a]^{1/a}, \quad (1)$$

where $M_{\max} = \mathbf{Clmax}$ and $a = \mathbf{Clpow}$ are tunable parameters of the hadronization model and $m_{1,2}$ are the constituent masses of the quarks $q_{1,2}$ inside the cluster in question. In this model, the kinematics of cluster fission

$$C(q_1, q_2) \rightarrow C_1(q_1, q), C_2(\bar{q}, q_2) \quad (2)$$

is determined by restricting the fission products to be aligned with the cluster axis along which the original quarks move back-to-back in the cluster rest frame. In this

fission a light $q\bar{q}$ pair with flavour $q \in \{u, d, s\}$ is drawn according to constant tunable relative weights \mathbf{Pwt}_q and the masses M_1 and M_2 of the children $C_{1,2}$ are usually drawn according to a power law,

$$(M_1 M_2)^{p-1}, \quad (3)$$

where $p = \mathbf{PSplit}$ is a further parameter of the model. The masses $M_{1,2}$ must of course be kinematically allowed, as the constituents carry masses. The value of p determines whether the children are rather heavy and slow, possibly leading to a longer chain of cluster fission until the threshold is reached, or whether a cluster quickly fissions into light and fast clusters. This will have a strong impact on the resulting multiplicity and spectra of hadrons. Once the masses $M_{1,2}$ are known, the momenta of all constituents can be determined, as also the new pair of quarks q is assumed to move along the cluster axis. Note that the phenomenological parameters M_{\max} , a and p are each a set of three parameters in **Herwig**, depending on whether the original cluster has a only $\{u, d, s\}$, c or b as constituents.

Once all clusters are fissioned they decay into pairs of hadrons. Here, once more a $q\bar{q}$ pair is drawn from the vacuum, such that two hadrons can form in pairs $H_1(q_1, q)$ and $H_2(\bar{q}, q_2)$. Note that also diquarks occur and hence the hadrons could be either mesons or baryons. All kinematically possible pairs of available hadrons are determined for every cluster and are assigned a weight that includes weight factors for angular momentum, flavour multiplet and phase space. Finally a pair is drawn according to these weights and the cluster decays isotropically into this hadron pair in its rest frame. Further details are described here [21].

In this work, we want to address two particular issues of this model. The first part is that the kinematics of cluster fission is strictly longitudinal along the cluster axis. On the other hand, the cluster decay is isotropic. This results in a hard transition from longitudinal to isotropic kinematics. Small transverse momentum smearing is only introduced via the cluster decay. If we view the cluster fission as a low-scale perturbative continuation of the parton shower this is once again a rather hard transition from soft and collinear dynamics to strictly longitudinal dynamics. Originally, these assumptions were made for simplicity in order not to attribute effects that should be determined by perturbative parton dynamics to the hadronization model. We will discuss these issues in the remainder of this work.

2.2 Hints from data

With new data on the production of identified particles we find hints that the hadronization model in its current implementation might have shortcomings. One example is the two-particle angular correlation of baryons as measured by the ALICE collaboration [22, 23].

Baryon production in the cluster hadronization model is usually achieved with the production of diquarks in intermediate steps. Originally, the only source of baryons, besides the remnants of the incoming hadrons, which are

a somewhat special case and not addressed here in particular, was the cluster decay into hadron pairs. Here, a mesonic cluster, i.e. a cluster made of a quark-antiquark pair, could decay into a pair of baryons by producing an intermediate pair of a diquark and anti-diquark of opposite flavour. As a result, baryon pairs are always strongly correlated in phase space as they always originate from the same cluster. A newer treatment of colour-reconnection in *Herwig* [24] has lead to some modification of this effect. Here, baryonic clusters, i.e. clusters made up of three quarks or three antiquarks, could arise from the colour rearrangement of nearby mesonic clusters. This leads to some decorrelation of baryon pairs.

However, this is not the final answer, as the correlation observables are found to also depend strongly on details of the cluster fission and decay. As an example we show in Fig. 3 ARGUS data at $\sqrt{s} = 10$ GeV e^+e^- collisions for baryon production only during the cluster decay (the default in *Herwig*) and only during the cluster fission. While the $p\bar{p}$ correlation data (upper panel) strongly favours cluster fission baryons, the baryon momentum spectrum data (lower panel) strongly favours the cluster decay baryons. These findings generalize also to high energy hadronic collisions. Therefore a deeper investigation of the interplay between cluster fission, cluster decay and colour reconnection is needed.

We will address the aforementioned colour reconnection effect, together with other effects in a forthcoming paper, which will complement the current study. This intertwined view on colour reconnection and dynamics of the cluster model already shows that it might be advantageous to consider these two effects in a more universal model. Such a model would address the non-perturbative evolution of momentum and colour degrees of freedom simultaneously. In this light, the current work should be regarded as another step towards a more universal model, and to provide hints to identify a number of observables which could constrain such an approach.

In this work we will address two closely related issues which both are the dynamical formulation of cluster fission and decay. In order to be able to address these processes in an unbiased way, we begin by disentangling the phase space for these processes from the actual dynamics that should be formulated as Lorentz-invariant matrix elements in both cases. For the cluster fission we will assume a perturbatively inspired matrix element that continues the perturbative evolution of the parton shower. The cluster decay ultimately needs to be derived within a framework of hadronic matrix elements. In our present work, we consider a more elaborate model than the isotropic decay in that we assume that the cluster to hadron transition is effectively governed by a t -channel type exchange with a non-perturbative matrix element.

As a guideline for the formulation of the model we keep in mind that the transitions between the different parts of the model should be smooth in order to reduce the dependence on intermediate scales. The cluster fission should be viewed as an evolution from an upper scale, the parton shower cutoff scale μ^2 towards a lower hadronic

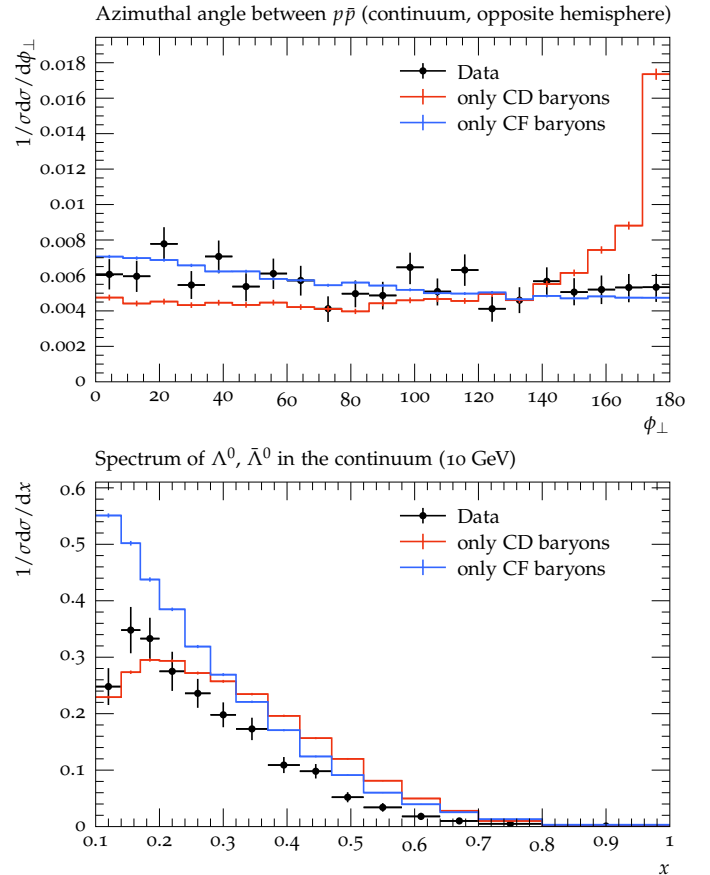


Fig. 3: The $p\bar{p}$ azimuthal angular correlations for e^+e^- collisions at $\sqrt{s} = 10$ GeV measured by ARGUS [25] for the opposite hemisphere (upper panel). ϕ_T is the angle between the transverse momenta with respect to the thrust axis, $\cos \phi_T = \hat{p}_{\perp,p} \cdot \hat{p}_{\perp,\bar{p}}$. Λ^0 baryon distribution of scaled momentum, $x = 2|\vec{p}|/\sqrt{s}$, measured by ARGUS [26] (lower panel).

scale, at which we transition to an initial condition which ultimately can only be determined non-perturbatively. We emphasise that this implies that if the parton shower evolution is stopped early, the cluster fission must act as a smooth continuation of the soft and collinear dynamics in the parton shower [18, 19], as illustrated in Fig. 1. Likewise, the cluster decay should pick up at the lower end of the cluster fission but has a discrete spectrum of hadron masses as lower bound and is therefore naturally regularized in its infrared region.

2.3 Phase space and matrix elements for cluster fission

In order to generically describe cluster fission in the aforementioned matrix element picture, we first employ the factorization of phase space in order to separate the pure phase space effects from the actual matrix element as depicted in Fig. 4. Those result from two assumptions by simply dissecting the relevant Feynman graphs: Clusters,

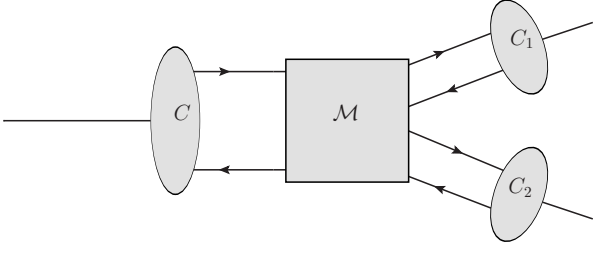


Fig. 4: Diagram of Cluster Fission

as imprinted by the nature of the external hadron amplitudes, essentially provide us with a 2-Particle-Irreducible (2PI) picture [18] in which we can organise the underlying Feynman graph using two-particle interaction diagrams as propagators of composite systems, which would also be removed in truncating for the use of external wave functions. We can then make the assumption that we effectively expand around on-shell quarks and gluons (on their constituent mass shell), while we currently neglect the four-point functions which evolve clusters into themselves.

We can write down a general $2 \rightarrow 4$ partonic process with a matrix element $\mathcal{M}_{2 \rightarrow 4}(p_1, p_2 \rightarrow q_1, q, \bar{q}, q_2)$, where the rate $\Gamma_{2 \rightarrow 4}$ can be written in this manner in $D = d + 1$ space-time dimensions:

$$\Gamma_{2 \rightarrow 4} = \int |\mathcal{M}_{2 \rightarrow 4}|^2 d\Phi_4 \quad (4)$$

$$d\Phi_4 = d\Pi_{q_1} d\Pi_q d\Pi_{\bar{q}} d\Pi_{q_2} (2\pi)^D \delta^D(p_1 + p_2 - \sum_f q_f) \quad (5)$$

$$d\Pi_{p_i} = \frac{d^d p_i}{(2\pi)^d 2E_{p_i}} \quad (6)$$

Note that in the above expression we choose the masses of the quarks to be the constituent masses instead of the current masses. This assumption was made since the cluster fission happens at a stage, where the current mass description breaks down. Otherwise, the cluster fission could lead to extremely light clusters. Rearranging the above expression we arrive at the following equation:

$$\begin{aligned} \Gamma_{2 \rightarrow 4} &\equiv \int dM_1 dM_2 f_{\text{PS}}(M_1, M_2) \\ &\quad d\Omega^{\text{COM}} d\Omega^{\text{COM},1} d\Omega^{\text{COM},2} |\mathcal{M}_{2 \rightarrow 4}|^2, \quad (7) \\ f_{\text{PS}}(M_1, M_2) &= \\ &\quad f_0 \frac{\sqrt{\lambda(M^2, M_1^2, M_2^2) \lambda(M_1^2, m_1^2, m_q^2) \lambda(M_2^2, m_2^2, m_q^2)}}{2M_1 M_2}, \quad (8) \end{aligned}$$

with a constant normalization factor f_0 and the Källén function $\lambda(x, y, z)$. Here, $f_{\text{PS}}(M_1, M_2)$ describes the mass distribution of clusters if the matrix element would have no implicit or explicit dependence on M_1, M_2 , i.e. the distribution coming purely from the 4-particle phase space.

mass phase space without matrix element
 $M = 10.58 \text{ GeV}$ and $m_1 = m_2 = m = 0.325 \text{ GeV}$

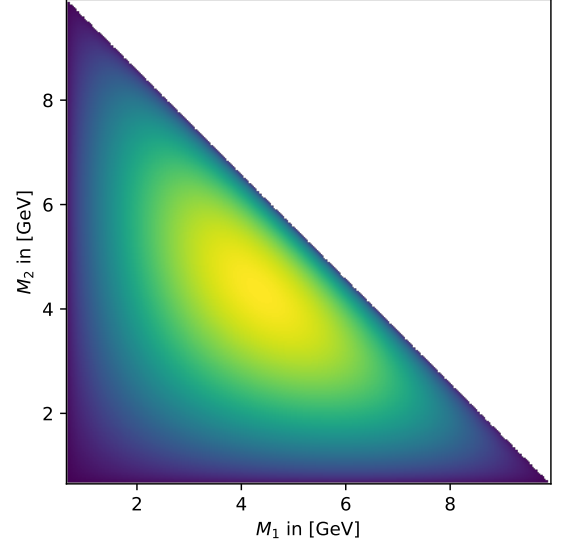


Fig. 5: Plot of flat mass phase space according to Eq. (8).

We define Ω^{COM} as the solid angle between the original constituent direction p_1 and the child cluster $Q_1 = (q_1 + q)$ in the rest frame of the original cluster. The solid angles $\Omega^{\text{COM},i}$ are the angles between the child cluster Q_i direction in the rest frame of the original cluster and q_i in the rest frame of Q_i respectively. We display the distribution $f_{\text{PS}}(M_1, M_2)$ in Fig. 5 for $m_1 = m_2 = m \equiv m_{u/d}$ at $M = \sqrt{s_{\text{BELLE}}}$, where $m_{u/d}$ is the constituent mass value of u/d quarks and $\sqrt{s_{\text{BELLE}}}$ is the COM energy of the BELLE experiment as we will later compare to BELLE data [27]. One can clearly note that the distribution in Fig. 5 is very different from a simple power law due to the threshold effects of the Källén functions in Eq. (8).

Note that Eq. (7) with a matrix element $|\mathcal{M}_{2 \rightarrow 4}|^2 = 1$ would sample the directions of clusters and their constituents completely isotropically. We rather want to extend the original picture of a strictly longitudinal cluster fission towards a picture that smoothly emerges from collinear emissions in the parton shower.

2.4 The Matrix Element

In order to achieve a non-trivial description of cluster fission that reflects the original picture of longitudinal fission as well as a smooth continuation of the parton shower evolution picture we make the following ansatz. As a cluster fission matrix element we choose a tree-level soft $q\bar{q}$ -emission, where a t -channel gluon exchange is needed in order to conserve momentum as shown in Fig. 6. A different way of viewing this exchange is the 2PI picture: we attach a cluster propagator in the lowest order together with the cluster branching matrix element. In order to simplify the matrix element, we employ the infra-red factorization from [28] to factorize the t -channel from the soft

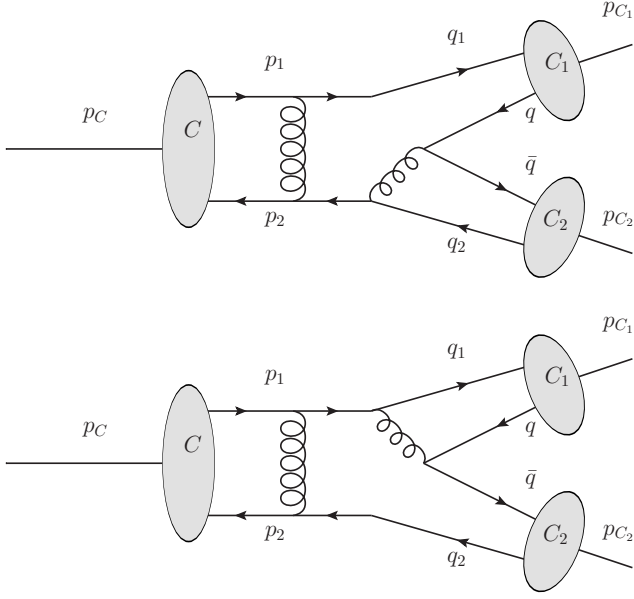


Fig. 6: Feynman diagrams of the chosen cluster fission matrix element.

function S , yielding in total the following:

$$|\mathcal{M}_{2 \rightarrow 4}|^2 = A_0 |\mathcal{M}_{2 \rightarrow 2}|_t^2 S(q_1, q_2, q, \bar{q}) \quad (9)$$

$$|\mathcal{M}_{2 \rightarrow 2}|_t^2 = \frac{(q_1 \cdot q_2)(p_1 \cdot p_2) + (q_1 \cdot p_2)(p_1 \cdot q_2)}{[(p_1 - q_1)^2 - \epsilon m_g^2][(p_2 - q_2)^2 - \epsilon m_g^2]} \quad (10)$$

It should be stressed that momentum conservation cannot usually be regarded a subleading effect within the realm of the hadronization model, and formally we should in fact consider next-to-leading power expansions of the factorized formulae. In the present work we do not consider the matrix element at this detailed level but rather make the assumption that energy-momentum conservation is properly implemented, and that the matrix element can actually be expressed in terms of particles “before” and “after” the emission, despite that the soft limit would normally not provide us with such an expression. A full derivation, including subleading-power effects, would be possible within the framework which has been sketched in [29], which is explicitly accounting for recoil and mass schemes within the factorization of matrix elements.

In addition to this, we need to address the infra-red divergence of the t -channel, which should be cancelled by the corresponding emission of a soft gluon of a $p_1 p_2$ -dipole. For the cluster model we put the gluons after the parton shower on a gluon constituent mass shell m_g . Hence, a reasonable regulator for our diagram shall be this gluon mass alongside with a parameter ϵ , which we choose to be 1 for all further considerations. In principle one could check the validity of the cancelling IR divergences, by varying the gluon constituent mass by a factor, but in practise this could inhibit some $g \rightarrow s\bar{s}$ splittings. Regarding future work, we want to mention that we will capture a partial effect of soft-gluon evolution colour reconnection,

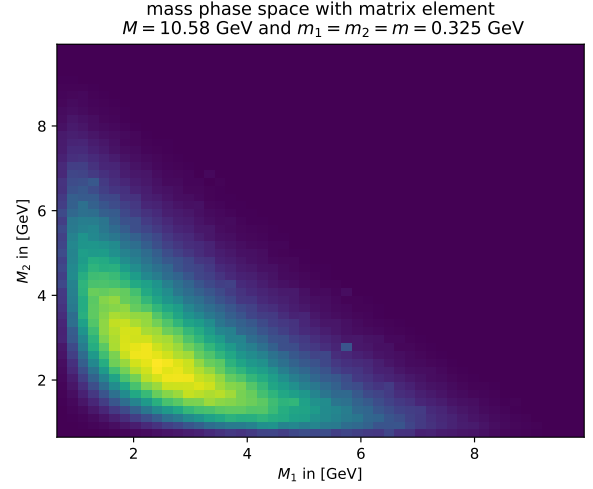


Fig. 7: Plot of mass phase space according to the matrix element.

which needs to be subtracted properly from the colour reconnection if one desires to interleave the two [20]. The soft function $S(q_1, q_2, q, \bar{q})$ consists of the following eikonal functions I_{ij} , which are defined as the following in [28]:

$$I_{ij}(p_i, p_j, q, \bar{q}) = \frac{(p_i \cdot q)(p_j \cdot \bar{q}) + (p_j \cdot q)(p_i \cdot \bar{q}) - (p_i \cdot p_j)(q \cdot \bar{q})}{(q \cdot \bar{q})^2 [p_i \cdot (q + \bar{q})] [p_j \cdot (q + \bar{q})]} \quad (11)$$

$$S(q_1, q_2, q, \bar{q}) = (I_{11} + I_{22} - 2I_{12}) \quad (12)$$

Note that we again explicitly break momentum conservation since in the soft limit $p_i \rightarrow q_i$, but in practise we have $p_i \neq q_i$. For the case at hand we choose q_1, q_2 for the soft function since we want to consider the matrix element shown in Fig. 6, where the $q\bar{q}$ -pair is emitted from the final state. The other convention was tried, but did not significantly impact the results. Furthermore we restored the mass dependence of the soft function by replacing $q \cdot \bar{q} \rightarrow q \cdot \bar{q} + m^2$, where $m^2 = q^2 = \bar{q}^2$.

This matrix element does not only have an impact on the directionality of cluster fission but also a significant contribution to the mass phase space. In particular the soft function has an explicit dependence on M_1, M_2 through the functions $I_{ij} \propto (M_i M_j + \dots)^{-2}$. This means that the matrix element impacts also the mass distributions of the clusters, which can be seen in Fig. 7, where we generated a weighted histogram of $\frac{1}{\Gamma_{2 \rightarrow 4}} \frac{d^2 \Gamma_{2 \rightarrow 4}}{dM_1 dM_2}$, which clearly differs from Fig. 5. The regulated poles of the soft function drive the masses down to lower values, while at the same time forbidding the region, where both clusters are light. As we want to sample also the angles efficiently, we found their distributions by using weighted histograms to be quite collinear as can be seen in Fig. 8. Note that here θ is the angle between p_1 and Q_1 , defined in the original cluster mass frame (COM) and θ_i are defined in the final cluster Q_i rest frame (COM $_i$) between the direction of Q_i in COM and q_i . For the normalized distribution $f_{\text{COM}}(\cos(\theta))$ we

assume the following type of distribution as a proposal distribution since this is motivated by the t -channel matrix element:

$$f_{\text{COM}}(\cos(\theta)) = \frac{A(2+A)}{[1+A-\cos(\theta)]^2} \quad (13)$$

Here $A > 0$ is a parameter of the distribution, which needs to be fitted to the histogram of the angle, which is plotted in Fig. 8. On the other hand for the $f_{\text{COM},i}(\cos(\theta_i))$ proposal distribution we choose an exponential ansatz which is motivated by the almost linear behaviour in the log plot of Fig. 8:

$$f_{\text{COM},i}(\cos(\theta_i)) = \frac{\beta_i}{1 - e^{-2\beta_i}} e^{\beta_i(\cos(\theta_i)-1)} \quad (14)$$

Here we choose $\beta_i > 0$ and fit this as well to the histograms at hand for obtaining the most efficient sampling later on.

These parameters A, β_1 and β_2 are of course in general functions of M, m_1, m_2, m , which complicates getting good overall efficiency in the rejection sampling, which we use later on. Of course if $m_1 = m_2$ this implies that $\beta_1 = \beta_2$.

2.5 Implementation of the algorithm in Herwig

In order to sample from Eq. (7) appropriately and with unit weights in **Herwig** we used the following algorithm for a single cluster fission:

1. **Flavour** — draw the flavour of the $q\bar{q}$ -pair using the default weights $\mathbf{Pwt}(q)$, which are constant parameters in **Herwig**.
2. **Cluster masses** — sample the masses M_1, M_2 uniformly in the allowed triangular phase space of Fig. 5
3. **Phase space** —
 - (a) Boost from the lab frame LAB to the centre of mass frame of the original cluster (COM)
 - (b) Sample the direction of the child clusters according to $f_{\text{COM}}(\cos(\theta))$
 - (c) Boost in both child cluster's rest frames (COM $_i$ for $i \in \{1, 2\}$) respectively
 - (d) Sample the direction of constituents according to $f_{\text{COM},i}(\cos(\theta_i))$ in the COM $_i$ frames
 - (e) Boost back to the original cluster rest frame COM
 - (f) Boost all momenta from to the COM frame to the LAB frame
4. Accept the configuration with P_{acc}

Note that we sample the masses M_1, M_2 uniformly, which - albeit not being the most efficient choice - is comparatively fast if the actual integrated mass distribution $\frac{1}{\Gamma_{2 \rightarrow 4}} \frac{d^2 \Gamma_{2 \rightarrow 4}}{dM_1 dM_2}$ is not known. Furthermore we always sample the azimuthal angles $\phi_{\text{COM}}, \phi_{\text{COM},1}$ and $\phi_{\text{COM},2}$ uniformly from $[0, 2\pi]$. Note that the two boosts in the points 3e - 3f are necessary since we cannot simply boost from the COM $_i$ frames to the LAB frame. Here, we would pick up a rotation since non-parallel Lorentz boosts do not commute. In the algorithm above we have to still define P_{acc} ,

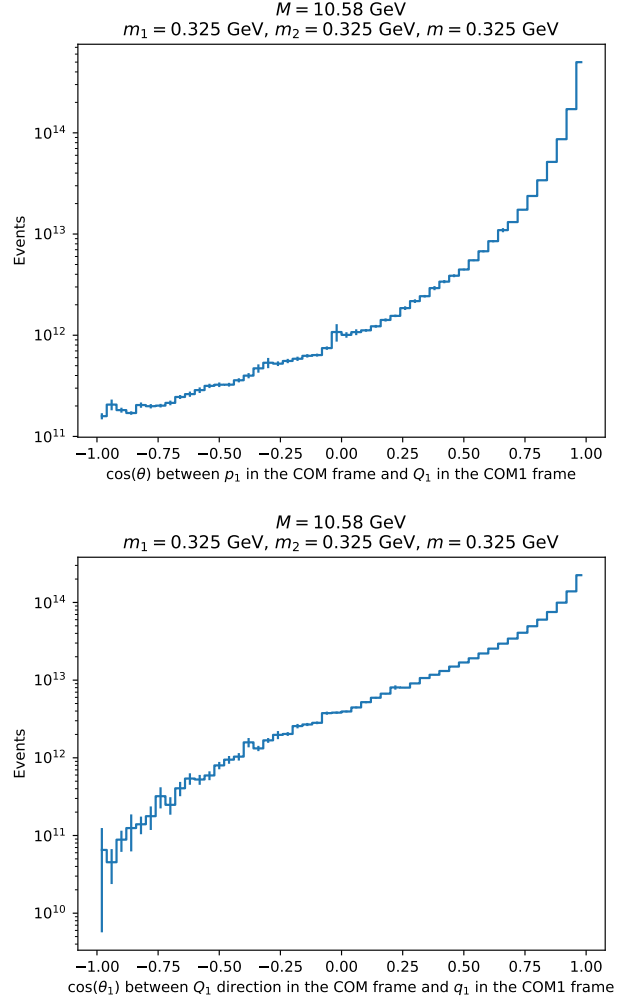


Fig. 8: Plot of distributions for angles according to the matrix element.

which we define as the following:

$$P_{\text{acc}} = \frac{f_{\text{PS}}(M_1, M_2) |\mathcal{M}|_{2 \rightarrow 4}^2(\{p_i \cdot p_j\})}{\lambda_{\text{OE}} f_{\text{MS}} f_{\text{COM}}(c_\theta) f_{\text{COM},1}(c_{\theta_1}) f_{\text{COM},2}(c_{\theta_2})} \quad (15)$$

Here we abbreviated $\cos(\theta_i) \equiv c_{\theta_i}$, $\{p_i \cdot p_j\}$ stands for the minimal set of all possible scalar products of the sampled set of four-momenta and λ_{OE} is the overestimate of the expression such that ideally $P_{\text{acc}} \leq 1$ for all phase space. In addition, f_{MS} could be a pre-sampler of the masses M_1, M_2 , but since we sample the masses uniformly we set $f_{\text{MS}} = 1$ without loss of generality. One should note that generally the best overestimate λ_{OE} is a function of M, m_1, m_2 and m . Furthermore, finding such an overestimate is highly non-trivial especially due to the denominator probability density functions. We therefore choose to get an estimate of the overestimate, by sampling the phase space and searching for a maximum of $\lambda_{\text{OE}} P_{\text{acc}}$ for fixed m_1, m_2 and m but variable M .

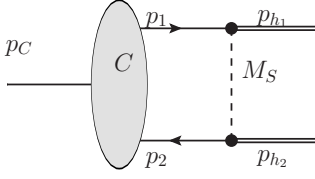


Fig. 9: Diagram of the chosen cluster decay matrix element. Currently we use this to sample the directions of the outgoing hadrons. In particular thresholds and the full mass dependence will be added later.

2.6 Phase space and matrix elements for cluster decay

The current cluster decay model of *Herwig* [4] forces clusters to decay to two hadrons, where the selection of a given hadron pair depends on different weight factors. These include a multiplicity factor for angular momenta, flavour multiplet weights for the individual hadrons and, most importantly a weight for the available phase space volume, which is given by the momentum of the decay products in the cluster rest frame, such that heavier hadrons are suppressed due to smaller momentum that would be available. Note, that baryons are treated separately from mesons, similar to the model in [30].

If a cluster cannot decay into two hadrons because its mass is too small to split into two hadrons a reshuffling with nearby clusters is performed and the cluster will be decayed to a single hadron. The kinematics of the decay are depending on whether at least one of the cluster's constituents have originated from the hard process or the parton shower and have a virtuality $q > m_g$, where $m_g = 0.95 \text{ GeV}$ is the gluon constituent mass, or the cluster has been produced during the cluster fission. In the latter case the cluster is decayed fully isotropically in its rest frame. In the first case the hadron directions $c_\theta = \cos(\theta_{p_1, h_1})$ (defined in the COM frame of the cluster with respect to the initial constituent partons) are sampled according to the distribution

$$f(c_\theta) = \frac{1}{\lambda} e^{\frac{c_\theta - 1}{\lambda}}. \quad (16)$$

This picture of treating clusters in a two-fold manner is contrary to the consequences from the colour evolution picture that the cluster fission should be treated perturbatively and the shower cutoff should be considered merely as a factorization scale [18].

We therefore present a new cluster decay model that tries to interpolate the cluster fission kinematics and the cluster decay kinematics in a more meaningful way. Similarly to the cluster fission, we assume a matrix element $\mathcal{M}_{p_1, p_2 \rightarrow h_1, h_2}$, which in this case is a $2 \rightarrow 2$ parton to hadron process. We choose a t -channel like interaction of the following form as displayed in Fig. 9:

$$\begin{aligned} |\mathcal{M}_{p_1, p_2 \rightarrow h_1, h_2}|^2 &= \frac{A_0}{[(p_1 - h_1)^2 - M_S^2]^2} \\ &= \frac{A'_0}{[A - \cos(\theta_{p_1, h_1})]^2} \end{aligned}$$

Here M_S is a pseudo mass parameter that we set to $M_S = \max\{(m_1 - m_{h_1}), (m_2 - m_{h_2})\}$ in order to have the maximally aligned cluster decay for small momentum constituents¹. A_0, A'_0 are arbitrary normalization constants.

While still a model assumption, the most important difference to the previous model obviously is the choice of kinematics and the t -channel behaviour. This will ensure a smooth continuation of the kinematics from the parton level into the hadron level. We will demonstrate the consequences of this choice below.

3 Impact on existing observables

Within the steps towards a new, evolving, hadronization model we are now mainly interested in finding observables which are able to help constrain the individual building blocks and where we can already see improvements from the modifications we propose. We will start by considering existing observables, and we limit ourselves to $e^+e^- \rightarrow q\bar{q}$ collision data such that multiple partonic interaction effects are absent and colour reconnection effects are not overpowering the cluster fission and decay effects that we want to study in this paper.

3.1 LEP energies

An obvious first test of the model is a comparison with data from LEP where most of the current hadronization models are tuned against particle yields and event shape data. In order to compare to experimental data we use the public analysis framework *Rivet* [32].

In Fig. 10 we show the distribution of transverse momenta relative to the thrust axis and the scaled momentum distribution at LEP for different cluster decay models and compare them to the ‘default’ *Herwig* model. Two of these choices are somewhat extreme. In the ‘aligned’ scheme the two hadrons move fully aligned with the original quarks. In the ‘isotropic’ scheme, the decay is fully isotropic which resembles the ‘default’ choice with the exception that also heavy quark containing clusters are fissioned completely isotropically.

Both observables show some sensitivity to the cluster decay model, especially for the low and high momentum regions. Nonetheless, we found that the new ‘ t -channel’ scheme – using the ansatz for a matrix element with a t -channel propagator as described in section 2.6 – does not introduce new tensions in the LEP observables. In fact, e.g. for the observables in Fig. 10 improvements with respect to the default model can be seen, where we should note that we left all other parameters at the tuned default values in order to highlight the differences between the model choices.

¹ Note that the maximum has to be taken since in general $p_1 \cdot h_1 > \max\{m_1 m_{h_1}, m_2 m_{h_2}\}$

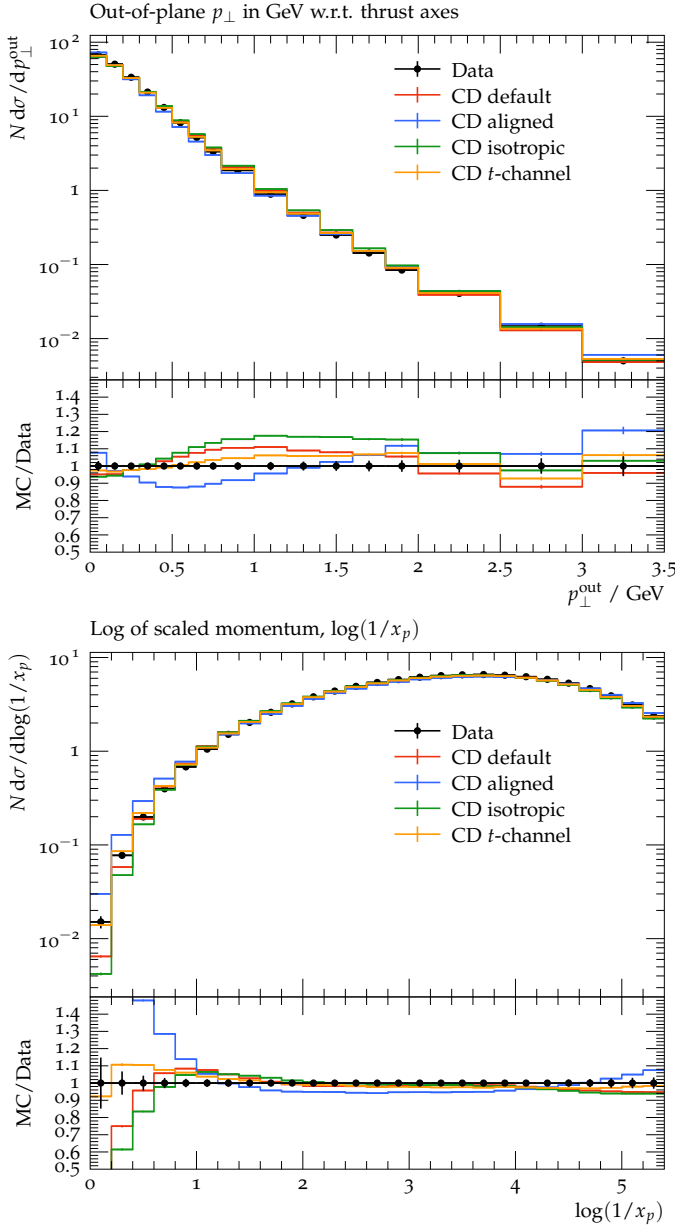


Fig. 10: The p_T^{out} distribution and the $\zeta_p = -\log x_p$ distribution measured by DELPHI [31], where $x_p = 2|\vec{p}|/\sqrt{s}$. We show a variation of different cluster decay models (keeping the *Herwig* default cluster fission), where ‘default’ is the *Herwig* default, ‘aligned’ is a fully aligned CD, ‘isotropic’ is a completely isotropic CD and t -channel is our matrix element ansatz for the CD.

3.2 Low energy e^+e^- data

Much more information will be available from data taken at lower energies, *e.g.* at B-factories, where the effect of the parton shower is small and in our picture the clusters are often formed directly by an initial $q\bar{q}$ system that will form a single primordial cluster that can decay, after one or at most very few possible fissions, into hadrons. In contrast, already at LEP the partons form jets and the properties

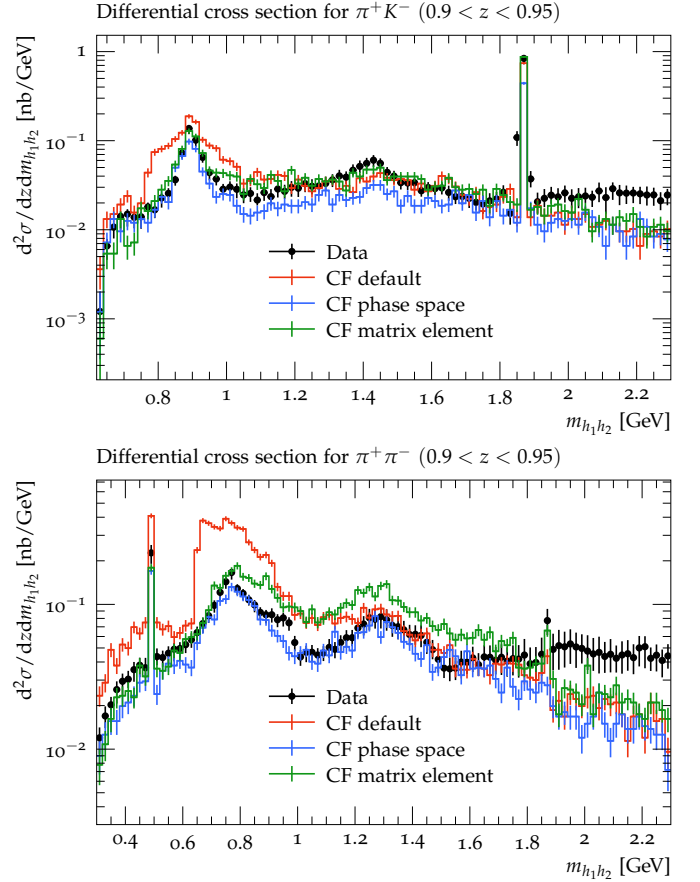


Fig. 11: Comparison of the different cluster fission models with respect to BELLE data from [33]. Here the t -channel like cluster decay was used.

of individual particle production only has a small effect on the properties of jet observables or event shapes.

We show some results of the newly proposed cluster fission algorithm for the di-hadron fragmentation function as a function of $m_{h_1h_2}$, binned in $z = 2(E_{h_1} + E_{h_2})/\sqrt{s}_{\text{BELLE}}$ measured by BELLE [33], where $m_{h_1h_2}$ is the invariant mass of two hadrons within the same event in the same hemisphere² and E_{h_i} is their respective energy. This observable is very sensitive to cluster fission for $z \rightarrow 1$ since in this case the parton shower is essentially not able to emit any partons above the parton shower cutoff and the particle production comes mostly from hadronization. Therefore, this region is dominated mostly by the recursive cluster fission of a $M_C \lesssim \sqrt{s}_{\text{BELLE}}$ mass cluster.

In Fig. 11 we compare the following three options for the cluster fission model, where for all of these the new t -channel like cluster decay model has been used:

1. *Herwig* 7.3.0. default fully aligned cluster fission (red)
2. The new model with the flat mass phase space and fully aligned fission (blue) according to Eq. (8)

² with respect to the thrust direction.

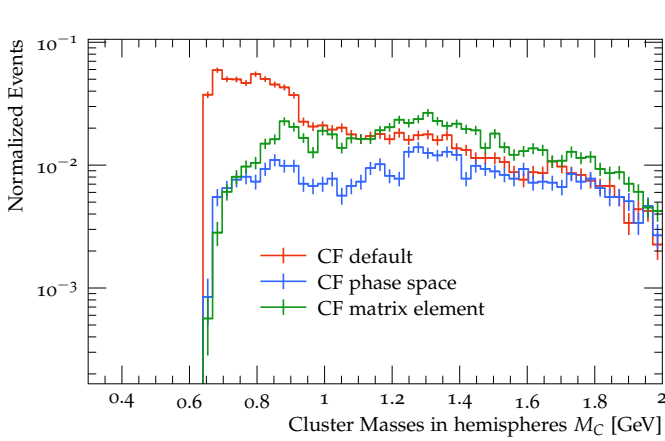


Fig. 12: The mass distribution of clusters binned in $\tilde{z} \in [0.9, 0.95]$. Here the t -channel like cluster decay was used.

3. The new model with the full matrix element dependence (green) and underlying mass distributions as shown in Fig. 7

We can clearly see that the **Herwig** ‘default’ forms a plateau starting from $(m_{q_1} + m_{q_2})$ until ~ 0.9 GeV, which can be explained by the fact that for **PSplit** ~ 1.0 the cluster mass distribution is a triangular distribution as also shown in [19]. This plateau is not reflected in the data, which hints at a breakdown of the default model for cluster fission. On the other hand we can see that the flat phase space and the full matrix element yield substantially better results except for the mid and high $m_{h_1 h_2}$ regions, where for the tail region none of the models describes the data accurately. The discrepancy in the mid region can be attributed at least partly to the fact that the new models are still untuned.

In Fig. 12 we plot the unphysical (but informative) cluster mass distribution $f(M_C)$ after the recursive cluster fission binned in $\tilde{z} = 2E_C/\sqrt{s}_{\text{BELLE}}$, where $E_C = E_1 + E_2$ is the energy of the cluster that decays into two hadrons of energies E_1 and E_2 . Looking at the cluster mass distributions one can clearly see that indeed the new cluster fission models are solving the plateau issue. In fact one can see that the hard turn-on of the cluster masses is regulated by the constituent masses of the quarks and the threshold functions of the phase space yielding to a smooth turn-on. This regularization of the infra-red divergence by massive partons is also a well-known feature of the parton shower.

We also examined the variation of the cluster decay model on these BELLE observables in Fig. 13, but with the exception of the extreme cases the impact of the cluster decay is rather limited.

4 Dissecting the hadronization history with new observables

As we have seen in the previous section some unphysical features could be successfully removed qualitatively, while

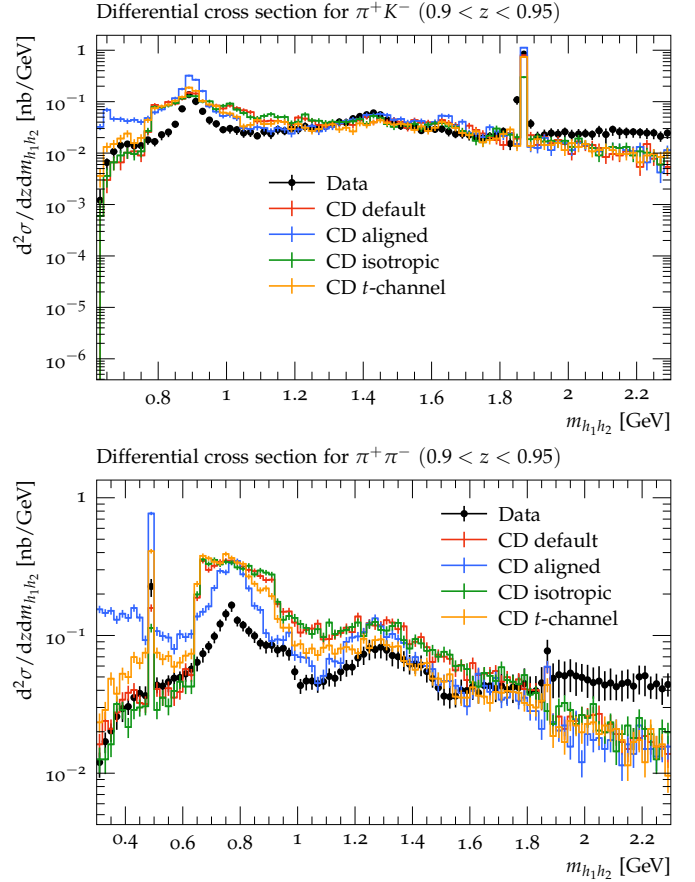


Fig. 13: Comparison of the different cluster decay models with respect to BELLE data from [33]. We used the default cluster fission model.

not producing different unphysical artefacts in other well established data. Nonetheless we want to study more in depth to which observables the cluster fission and the cluster decay model are most sensitive. To this end we present in this section phenomenological studies of the generalized jet angularities and the multi point energy correlators. Since we want to find classes of observables that can be sensitive to both cluster fission and cluster decay we show in the following only observables at $\sqrt{s} = M_Z$ unless stated otherwise.

4.1 Angularities

In addition to the improved behaviour for the measured observables in Fig. 10 and Fig. 11 we also show generalized angularities and multi-energy correlations, which are sensitive to the different stages of hadronization. The generalized angularities λ_β^α introduced in [34, 35] are defined as

$$\lambda_\beta^\alpha = \sum_{i \in \{\text{jet}\}} z_i^\beta \theta_i^\alpha, \quad (17)$$

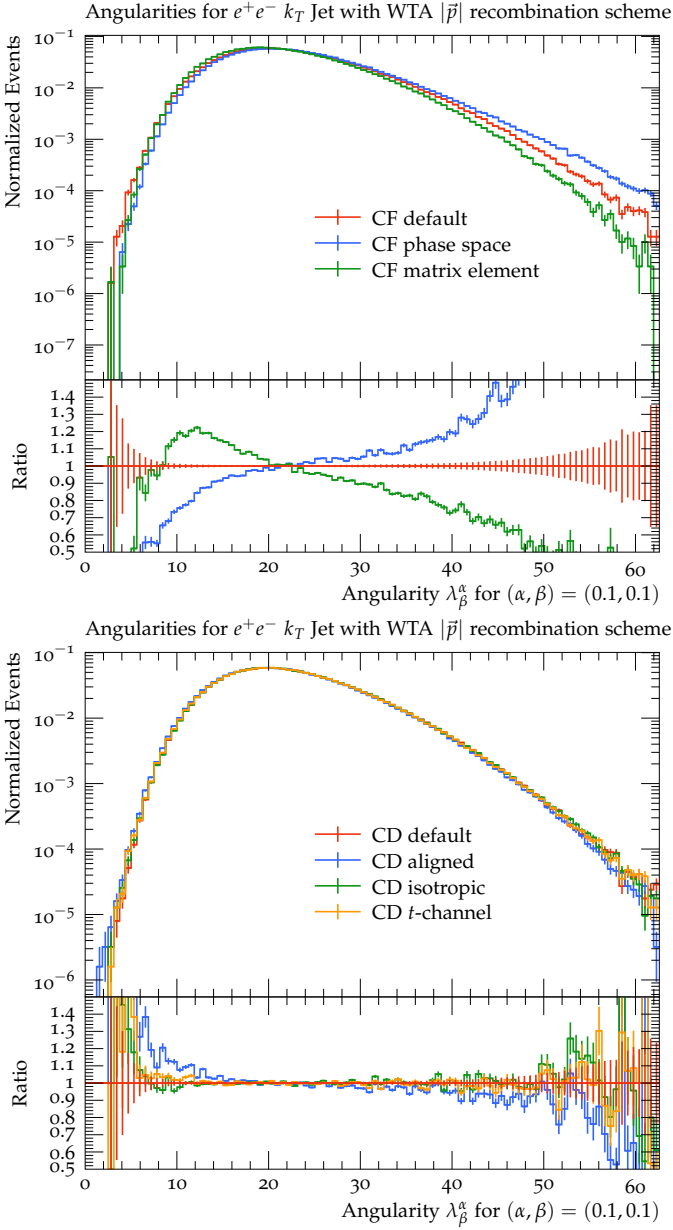


Fig. 14: The generalized jet angularities for $\alpha = 0.1, \beta = 0.1$ for the k_t WTA algorithm. We show a variation of the cluster fission models with the t -channel like cluster decayer (top) and the different cluster decay models with the *Herwig* default cluster fission (bottom).

where $\theta_i := \sqrt{2(1 - \cos(\hat{\theta}_i))}$ is defined with $\hat{\theta}_i$ being the angle between jet constituent i and the jet. The energy fraction $z_i = \frac{E_i}{E_{\text{vis}}}$ is defined as $E_{\text{vis}} = \sum_{i \in \{\text{event}\}} E_i$ and gives a measure of hardness. Different powers of β and α provide different weighting of softness and collinearity respectively and give insights into different regimes of the infra-red and collinear limit. Note in particular that the angularities λ_β^α are infra-red safe for $\beta > 0$ and additionally collinear safe if $\beta = 1$ and $\alpha \geq 0$. As a jet algorithm we used the generalized k_T algorithm with the Winner-

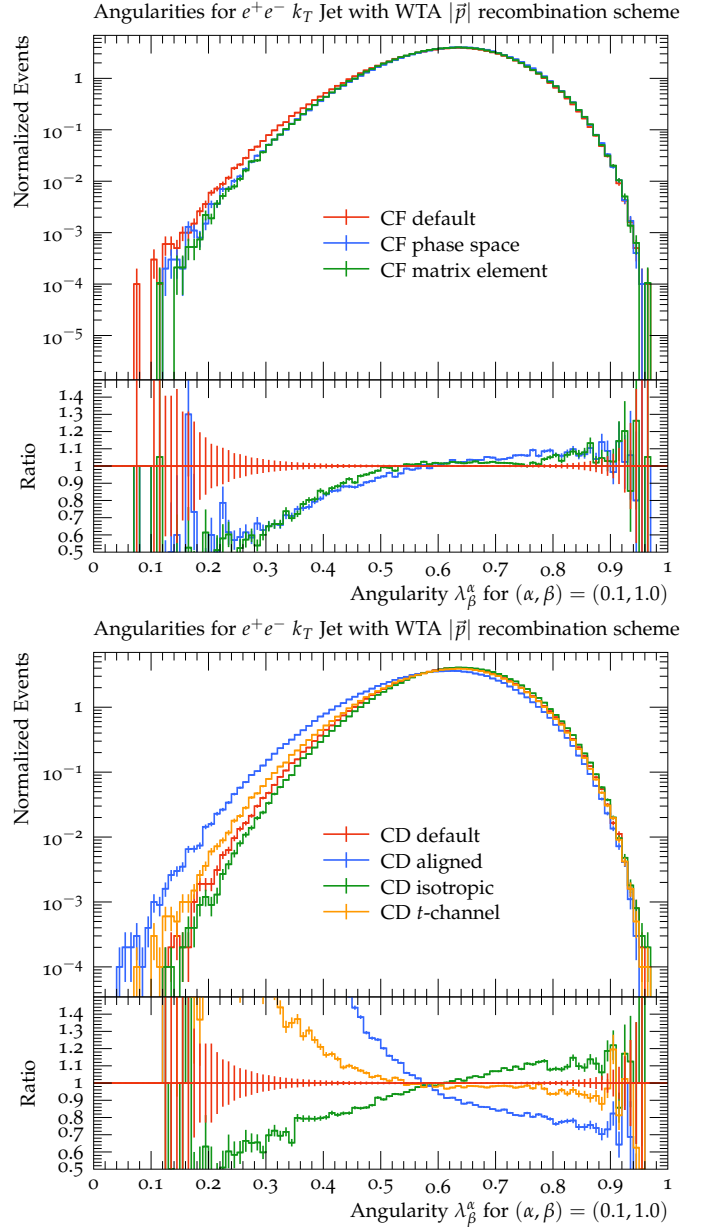


Fig. 15: The generalized jet angularities for $\alpha = 0.1, \beta = 1.0$ for the k_T WTA algorithm. We show a variation of the cluster fission models with the t -channel like cluster decayer (top) and the different cluster decay models with the *Herwig* default cluster fission (bottom).

Takes-All (WTA) $|\vec{p}|$ -recombination scheme [36, 37] from *FastJet* [38] to cluster each event into 2 exclusive jets.

In Fig. 14 and Fig. 15 we show various generalized angularities for the case of e^+e^- collisions at $\sqrt{s} = M_Z$. In particular we compare different cluster fission models on top and different cluster decay models on the bottom for $\alpha = 0.1$ and different β . We can clearly see that in Fig. 14 the cluster decay model is irrelevant, but the cluster fission model has a strong impact on the observable. This can be attributed to the fact that in the limit $\alpha, \beta \rightarrow 0$ the angularities become the jet multiplicity and since only the

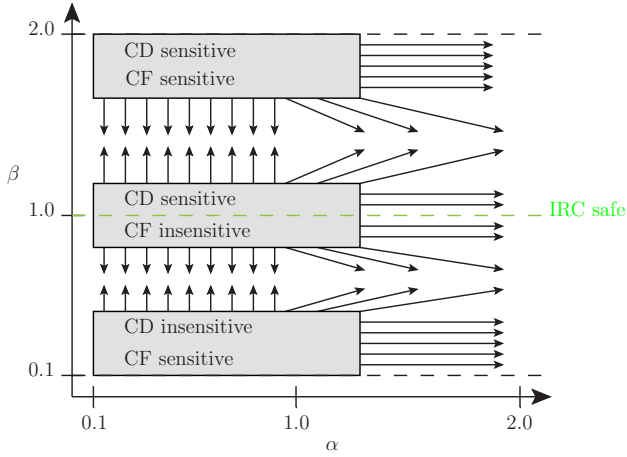


Fig. 16: Summary sketch of the angularity parameter space of α, β with its corresponding sensitivities to the cluster fission and cluster decay. The arrows point towards decreasing sensitivities and the boxes represent the regions with the most sensitivity and discriminative power.

cluster fission can produce multiplicity, the cluster decay is irrelevant to this observable. In Fig. 15 we see the opposite behaviour i.e. the cluster decay has a strong impact on the observable, while the cluster fission has only limited impact on the observable.

We have studied several different values in the (α, β) space and summarize our findings in the sketch Fig. 16, where we show the regions with the most sensitivity as grey blocks and the arrows point towards decreasing sensitivity in general. It is remarkable that the cluster fission model shows the least sensitivity in Fig. 15, i.e. for the collinear safe angularities, while the cluster decay has a huge impact on this observable. Note that this observable in the limit $\alpha \rightarrow 0$ is just the energy fraction of the jet.

4.2 Correlations

In addition to the angularities we looked at weighted multi-point energy correlations $\text{ENC}_\gamma(\theta)$, which are defined as

$$\text{ENC}_\gamma(\theta) = \frac{1}{\sigma_{\text{tot}}} \sum_{m=N}^{\infty} \int d\sigma_m \mathcal{W}_m^\gamma[\theta, \{p_i\}_m] \quad (18)$$

$$d\sigma_m = d\sigma(e^+e^- \rightarrow p_1, \dots, p_m) \quad (19)$$

$$\mathcal{W}_m^\gamma[\theta, \{p_i\}_m] = \frac{1}{D_m^\gamma} \sum_{i_1 < \dots < i_N}^m \left(\prod_{k=1}^N E_{i_k}^\gamma \right) \delta(\hat{\theta}(\{\hat{p}_{i_k}\}_N) - \theta) \quad (20)$$

$$D_m^\gamma = \sum_{i_1 < \dots < i_N}^m \left(\prod_{k=1}^N E_{i_k}^\gamma \right). \quad (21)$$

Here, $\hat{\theta}(\{\hat{p}_i\}_N)$ is a symmetric function of the N particle directions on the subset $\{p_i\}_N \subseteq \{p_i\}_m$ of the m particle final state $\{p_i\}_m$. Note that the N -point correlations

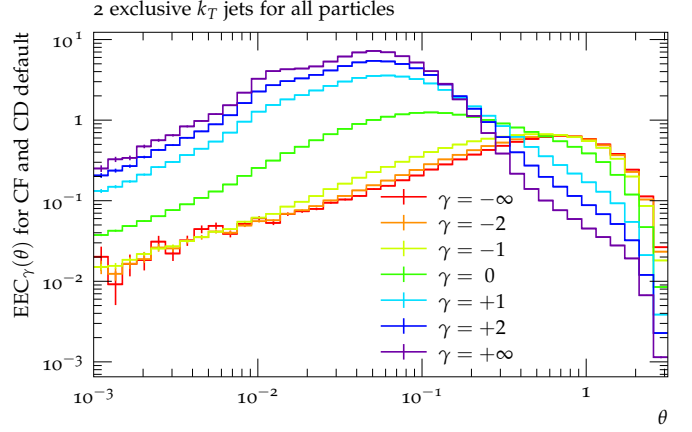


Fig. 17: We show the $\text{EEC}(\theta)$ correlation of two exclusive k_T jets for variable γ with the default cluster fission and cluster decay model.

$\text{ENC}_\gamma(\theta)$ are normalized to unity, with the total inclusive cross section $\sigma_{\text{tot}} \equiv \sum_{m=2}^{\infty} \sigma_m$. Due to the computational cost, which is $\mathcal{O}(m^N)$, of the $\text{ENC}_\gamma(\theta)$ for large m we limit ourselves to the cases $N \in \{2, 3\}$. For $N = 2$ the regular infrared safe energy-energy correlations are recovered if the function $\hat{\theta}(\hat{p}_1, \hat{p}_2) \equiv \theta_{12}$ and $\gamma = 1$ is chosen, but since we are not reliant on any infrared safety condition the value of γ can be an arbitrary real number and in particular also negative values, which would lead to an *infrared dangerous* observable. In this study we looked at the values $\gamma \in \{0, \pm 1, \pm 2, \pm \infty\}$, even though fractional values are also possible. We call $\gamma \rightarrow +\infty$ the ‘Winner-Takes-All’ (WTA) correlation and $\gamma \rightarrow -\infty$ the ‘Soft-Takes-All’ (STA) correlation, which corresponds to filling only the largest product of energies per event for WTA (smallest for STA).

In practise we find that the correlations for any finite γ we studied are qualitatively similar to an interpolation between the WTA and STA correlations as we show e.g. in Fig. 17 for the observable $\text{EEC}(\theta)$. Therefore, we only consider the WTA and STA correlations as most extreme cases in the following.

While for $N = 2$ we choose the relative angle θ_{ij} between the two particles in the lab frame, for $N = 3$ we choose the function $\hat{\theta}(\hat{p}_1, \hat{p}_2, \hat{p}_3)$ as the minimum and maximum of the pair-wise relative angles θ_{ij} :

$$\hat{\theta}_{\min}(\hat{p}_1, \hat{p}_2, \hat{p}_3) = \min_{i < j} \{\theta_{ij}\} \quad (22)$$

$$\hat{\theta}_{\max}(\hat{p}_1, \hat{p}_2, \hat{p}_3) = \max_{i < j} \{\theta_{ij}\} \quad (23)$$

Note that neither the choice of $\hat{\theta}_{\min}$ or $\hat{\theta}_{\max}$ is a collinear safe choice since we let the sum in Eq. (20) run over distinct ordered tuples of particles instead of all possible tuples (compare e.g. [39]). However in the quest for studying soft physics we are not limited to collinear safe observables either.

In addition to the inclusive final state energy correlations we looked at energy correlations within two exclusive

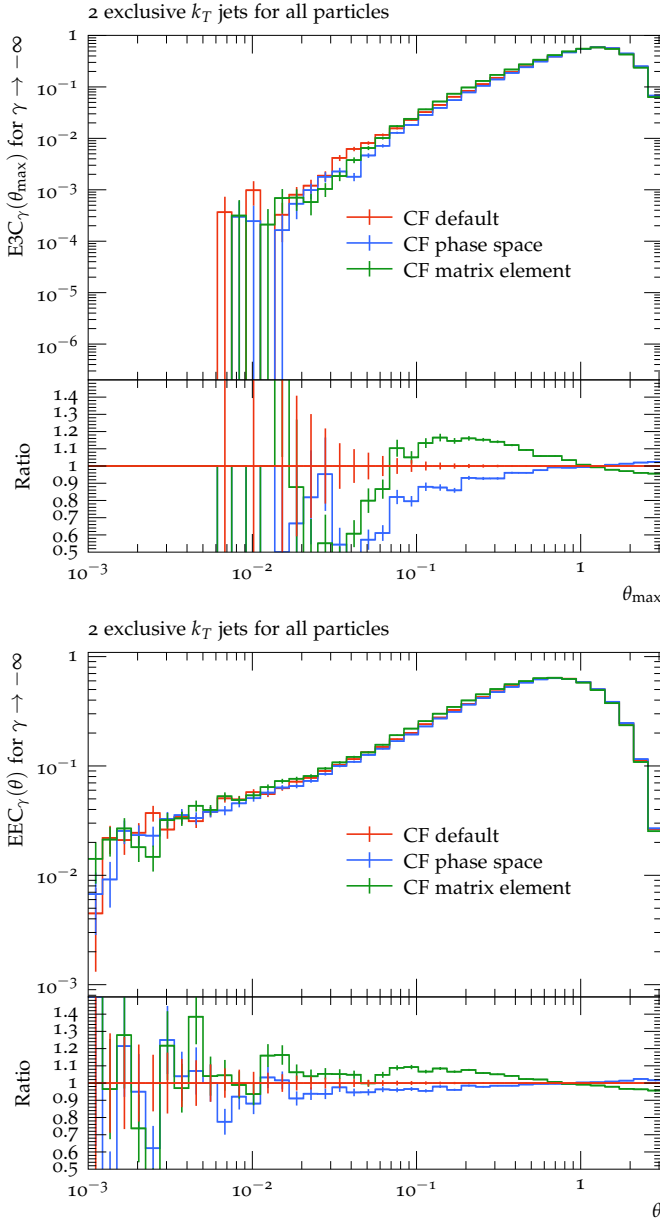


Fig. 18: The STA ($\gamma \rightarrow -\infty$) energy correlator $E3C_\gamma(\theta_{\max})$ (top) and $EEC_\gamma(\theta)$ (bottom) of two exclusive k_T jets. We show a variation of the cluster fission models with the t -channel like cluster decayer.

jets clustered using the Durham k_T algorithm [40] with the E recombination scheme. For this we computed the ENC_γ on the set of particles within each jet and scaled the overall observable by the number of jets, here two, such that the normalization to unity is recovered.

In Fig. 18 we display the STA $E3C_\gamma(\theta_{\max})$ and $EEC_\gamma(\theta)$ for a variation of the cluster fission model with the t -channel like cluster decayer. We note that the observable is sensitive to the choice of the cluster fission model. The same observables were studied for fixed cluster fission and variable cluster decay model, which showed that they were not at all dependent on the cluster decay. In fact, all the

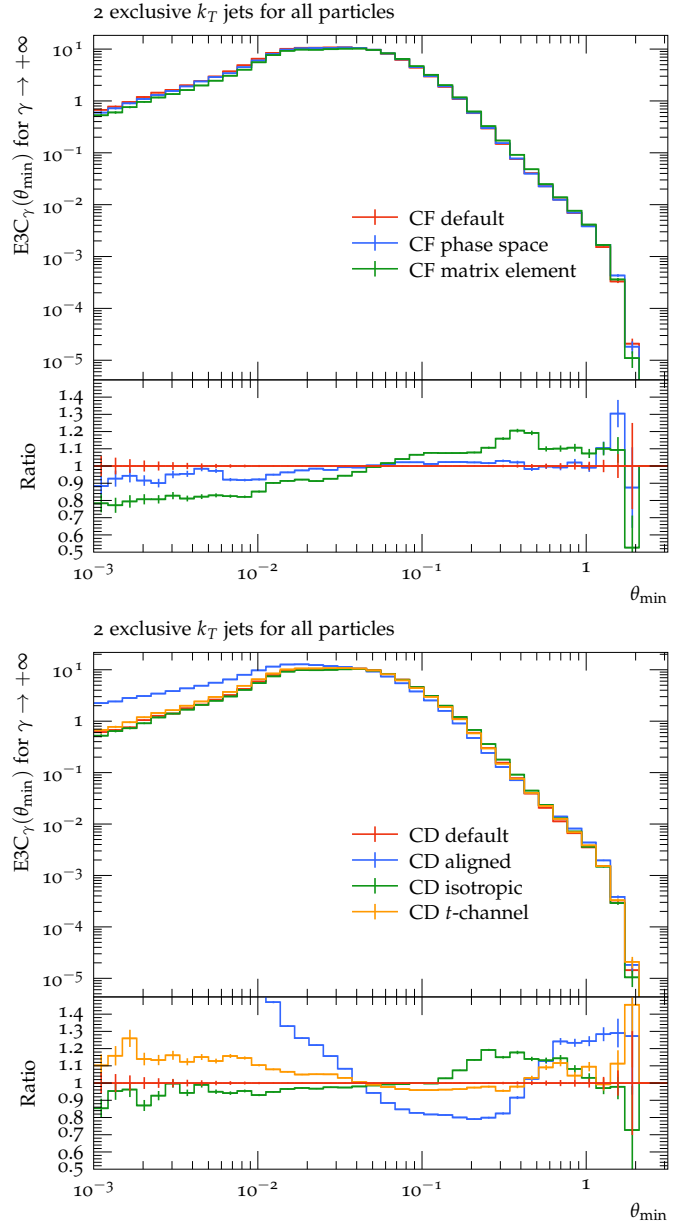


Fig. 19: The WTA ($\gamma \rightarrow +\infty$) energy correlator $E3C_\gamma(\theta_{\min})$ of two exclusive k_T jets. We show a variation of the cluster fission models with the t -channel like cluster decayer (top) and the different cluster decay models with the *Herwig* default cluster fission (bottom).

STA energy correlations we studied were essentially oblivious to the cluster decay model. This observation implies that these STA correlations are able to discriminate between different cluster fission models but at the same time they are not affected by the cluster decay model.

In contrast, for the WTA $E3C_\gamma(\theta_{\min})$ correlations, which we show in Fig. 19, sensitivity to both cluster fission (top) and cluster decay (bottom) can be observed. In Fig. 20 we show the WTA $EEC(\theta)$ correlations for different cluster fission models (top) and different cluster decay models (bottom). As one can clearly see, both are sensi-

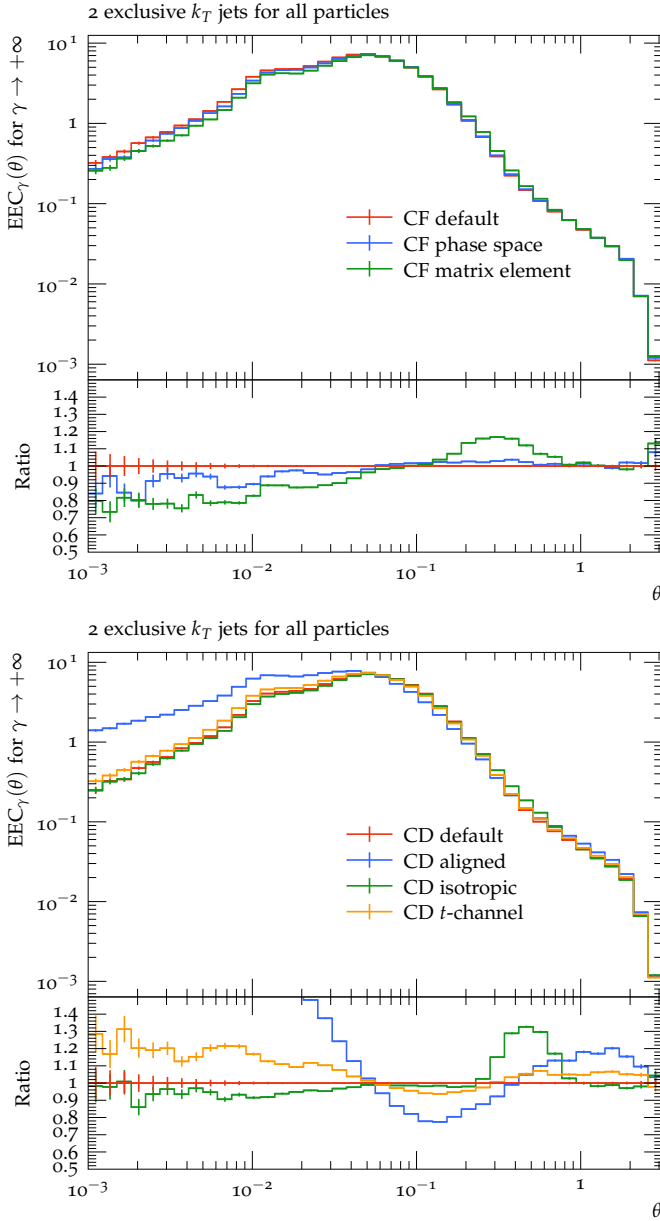


Fig. 20: The WTA ($\gamma \rightarrow +\infty$) energy correlator $EEC_\gamma(\theta)$ of two exclusive k_T jets. We show a variation of the cluster fission models with the t -channel like cluster decayer (top) and the different cluster decay models with the *Herwig* default cluster fission (bottom).

tive to this observable, but the cluster fission has almost no impact at large angles $\theta > 1$, while the cluster decay is significantly sensitive. Note that the smaller secondary bump at $\theta \simeq 10^{-2}$ comes from the hadron decay model.

To assess the dependence of these correlations on different centre of mass energies \sqrt{s} , we compare the STA and WTA energy correlations $EEC_\gamma(\theta)$ for two different $\sqrt{s} \in \{\sqrt{s}_{\text{BELLE}}, M_Z\}$ in Fig. 21. One can clearly see that for the STA correlations the distributions look quite similar, as one would expect, since this observable is infrared dangerous, i.e. the addition of a hard particle to the

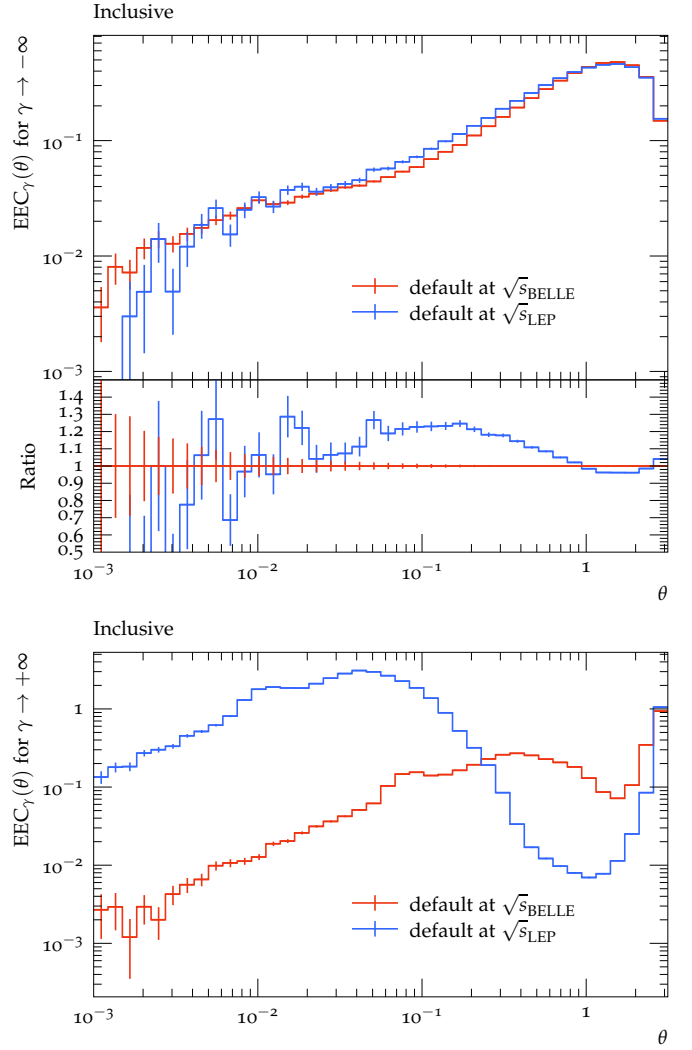


Fig. 21: The STA (top) and WTA (bottom) energy correlators $EEC_\gamma(\theta)$ inclusive over the whole event for $\sqrt{s} \in \{10.58 \text{ GeV}, 91.2 \text{ GeV}\}$. Both plots are made with the *Herwig* default cluster fission and decay.

event does not change³ the observable. In other words, this observable measures the soft structure of a fragmenting unbound $q\bar{q}$ state produced at energies \sqrt{s} , which is independent of the hard scale \sqrt{s} if hadronization universality is assumed. The residual difference between the two lines can be partly attributed to the hadronization power corrections of $\mathcal{O}(\Lambda_{\text{QCD}}/\sqrt{s})^p$.

On the other hand we show the WTA correlations in Fig. 21. In this case of course we expect large differences since the observable is IR safe and thus very sensitive to the hard scale \sqrt{s} . One can see that the collinear peak shifts to lower angles for higher energies.

³ In principle, an infinitely hard particle, but one can rephrase this as rescaling all other particles to become infinitely soft.

5 Conclusion and Outlook

In the present study we have started to build a novel structure for the cluster hadronization model, which is driven by low-scale perturbative processes driving the cluster fission and eventually non-perturbative cluster decays. We have in particular focused on determining observables which will be sensitive to such building blocks and can complement theoretical considerations on how to build such a model. We also emphasize that explicitly infrared unsafe – and in particular infrared dangerous – observables should complement the tuning of hadronization models and can be constructed in a way that they are insensitive to hard physics, and maximally sensitive to hadronization within different ranges of relevant scales. Our approach will be unified with a similar view on colour reconnection, based on exploratory steps in [20], and as a unique consequence of the evolution equations proposed in [18].

Our present analysis is in line with some of the motivations presented in [19], and able to generalize this approach towards a more universal model. We emphasize that the construction of the dynamic model can benefit from the class of observables we have developed here, and that we should ultimately seek to construct a new model which would include gluons and quarks as cluster constituents on the same footing. In fact, infrared safety in a more general sense as presented in [18], does imply that this needs to be the case. In particular, a closer link to re-organizing the low-scale perturbative Feynman graphs is possible within our paradigm, and has motivated us to use a 2PI picture (*i.e.* one in which two-body interactions of constituents define propagators of internal systems, and which will be removed when truncating Green's functions) to identify the cluster fission matrix elements. Our analysis needs to be completed by including cluster propagators, and then ultimately allows us to leverage input from Bethe-Salpeter amplitudes to construct a model in which more building blocks can be obtained from first principles.

Acknowledgments

We would like to thank Gernot Eichmann, Massimiliano Procura, Daniel Samitz and Wouter Waalewijn for fruitful discussions.

This work has been supported in part by the BMBF under grant agreements BMBF 05H21VKCCA and 05H24VKB. S.K. acknowledges the support through a KHYS travel grant and the kind hospitality of the Institute of Physics of the NAWI Graz.

References

1. J. Bellm et al., *Herwig 7.0/Herwig++ 3.0 release note*, *Eur. Phys. J. C* **76** (2016), no. 4 196, [[arXiv:1512.01178](#)].
2. J. Bellm et al., *Herwig 7.1 Release Note*, [arXiv:1705.06919](#).
3. J. Bellm et al., *Herwig 7.2 release note*, *Eur. Phys. J. C* **80** (2020), no. 5 452, [[arXiv:1912.06509](#)].
4. G. Bewick et al., *Herwig 7.3 release note*, *Eur. Phys. J. C* **84** (2024), no. 10 1053, [[arXiv:2312.05175](#)].
5. C. Bierlich et al., *A comprehensive guide to the physics and usage of PYTHIA 8.3*, *SciPost Phys. Codeb.* **2022** (2022) 8, [[arXiv:2203.11601](#)].
6. Sherpa Collaboration, E. Bothmann et al., *Event generation with Sherpa 3*, *JHEP* **12** (2024) 156, [[arXiv:2410.22148](#)].
7. M. Dasgupta, F. A. Dreyer, K. Hamilton, P. F. Monni, G. P. Salam, and G. Soyez, *Parton showers beyond leading logarithmic accuracy*, *Phys. Rev. Lett.* **125** (2020), no. 5 052002, [[arXiv:2002.11114](#)].
8. J. R. Forshaw, J. Holguin, and S. Plätzer, *Building a consistent parton shower*, *JHEP* **09** (2020) 014, [[arXiv:2003.06400](#)].
9. Z. Nagy and D. E. Soper, *Summations of large logarithms by parton showers*, *Phys. Rev. D* **104** (2021), no. 5 054049, [[arXiv:2011.04773](#)].
10. F. Herren, S. Höche, F. Krauss, D. Reichelt, and M. Schoenherr, *A new approach to color-coherent parton evolution*, *JHEP* **10** (2023) 091, [[arXiv:2208.06057](#)].
11. M. van Beekveld, S. Ferrario Ravasio, G. P. Salam, A. Soto-Ontoso, G. Soyez, and R. Verheyen, *PanScales parton showers for hadron collisions: formulation and fixed-order studies*, *JHEP* **11** (2022) 019, [[arXiv:2205.02237](#)].
12. S. Höche, F. Krauss, and D. Reichelt, *The Alaric parton shower for hadron colliders*, [arXiv:2404.14360](#).
13. M. van Beekveld et al., *New Standard for the Logarithmic Accuracy of Parton Showers*, *Phys. Rev. Lett.* **134** (2025), no. 1 011901, [[arXiv:2406.02661](#)].
14. S. Plätzer, *Summing Large- N Towers in Colour Flow Evolution*, *Eur. Phys. J. C* **74** (2014), no. 6 2907, [[arXiv:1312.2448](#)].
15. J. R. Forshaw, J. Holguin, and S. Plätzer, *Parton branching at amplitude level*, *JHEP* **08** (2019) 145, [[arXiv:1905.08686](#)].
16. M. De Angelis, J. R. Forshaw, and S. Plätzer, *Resummation and Simulation of Soft Gluon Effects beyond Leading Color*, *Phys. Rev. Lett.* **126** (2021), no. 11 112001, [[arXiv:2007.09648](#)].
17. J. R. Forshaw, S. Plätzer, and F. T. González, *Exact colour evolution for jet observables*, [arXiv:2502.12133](#).
18. S. Plätzer, *Colour evolution and infrared physics*, *JHEP* **07** (2023) 126, [[arXiv:2204.06956](#)].
19. A. H. Hoang, O. L. Jin, S. Plätzer, and D. Samitz, *Matching Hadronization and Perturbative Evolution: The Cluster Model in Light of Infrared Shower Cutoff Dependence*, [arXiv:2404.09856](#).
20. S. Gieseke, P. Kirchgaßer, S. Plätzer, and A. Siodmok, *Colour Reconnection from Soft Gluon Evolution*, *JHEP* **11** (2018) 149, [[arXiv:1808.06770](#)].
21. M. Bahr et al., *Herwig++ Physics and Manual*, *Eur. Phys. J. C* **58** (2008) 639–707, [[arXiv:0803.0883](#)].
22. ALICE Collaboration, J. Adam et al., *Insight into particle production mechanisms via angular correlations of identified particles in pp collisions at $\sqrt{s} = 7$ TeV*, *Eur. Phys. J. C* **77** (2017), no. 8 569, [[arXiv:1612.08975](#)]. [Erratum: *Eur. Phys. J. C* **79**, 998 (2019)].
23. ALICE Collaboration, S. Acharya et al., *Studying strangeness and baryon production mechanisms through*

- angular correlations between charged Ξ baryons and identified hadrons in pp collisions at $\sqrt{s} = 13$ TeV*, [arXiv:2308.16706](#).
24. S. Gieseke, P. Kirchgaesser, and S. Plätzer, *Baryon production from cluster hadronisation*, [Eur. Phys. J. C](#) **78** (2018), no. 2 99, [[arXiv:1710.10906](#)].
 25. **ARGUS** Collaboration, H. Albrecht et al., *Results on Baryon anti-Baryon Correlations in e^+e^- Annihilation*, [Z. Phys. C](#) **43** (1989) 45.
 26. **ARGUS** Collaboration, H. Albrecht et al., *Hyperon Production in e^+e^- Annihilation at 10-GeV Center-of-mass Energy*, [Z. Phys. C](#) **39** (1988) 177.
 27. **Belle** Collaboration, S. L. Olsen, *The BELLE experiment at KEKB*, in 1994 Meeting of the American Physical Society, Division of Particles and Fields (DPF 94), pp. 1908–1913, 8, 1994.
 28. S. Catani and M. Grazzini, *Infrared factorization of tree level QCD amplitudes at the next-to-next-to-leading order and beyond*, [Nucl. Phys. B](#) **570** (2000) 287–325, [[hep-ph/9908523](#)].
 29. S. Plätzer and M. Sjodahl, *Amplitude factorization in the electroweak standard model*, [Phys. Rev. D](#) **110** (2024), no. 5 056023, [[arXiv:2204.03258](#)].
 30. A. Kupco, *Cluster hadronization in HERWIG 5.9*, in [Workshop on Monte Carlo Generators for HERA Physics \(Plenary Starting Meeting\)](#), pp. 292–300, 4, 1998. [[hep-ph/9906412](#)].
 31. **DELPHI** Collaboration, P. Abreu et al., *Tuning and test of fragmentation models based on identified particles and precision event shape data*, [Z. Phys. C](#) **73** (1996) 11–60.
 32. C. Bierlich, A. Buckley, J. Butterworth, C. H. Christensen, L. Corpe, D. Grellscheid, J. F. Grosse-Oetringhaus, C. Gutsche, P. Karczmarczyk, J. Klein, L. Lönnblad, C. S. Pollard, P. Richardson, H. Schulz, and F. Siegert, *Robust independent validation of experiment and theory: Rivet version 3*, [SciPost Physics](#) **8** (Feb., 2020).
 33. **Belle** Collaboration, R. Seidl et al., *Invariant-mass and fractional-energy dependence of inclusive production of di-hadrons in e^+e^- annihilation at $\sqrt{s} = 10.58$ GeV*, [Phys. Rev. D](#) **96** (2017), no. 3 032005, [[arXiv:1706.08348](#)].
 34. P. Gras, S. Höche, D. Kar, A. Larkoski, L. Lönnblad, S. Plätzer, A. Siódmok, P. Skands, G. Soyez, and J. Thaler, *Systematics of quark/gluon tagging*, [JHEP](#) **07** (2017) 091, [[arXiv:1704.03878](#)].
 35. A. J. Larkoski, I. Moulton, and D. Neill, *Toward Multi-Differential Cross Sections: Measuring Two Angularities on a Single Jet*, [JHEP](#) **09** (2014) 046, [[arXiv:1401.4458](#)].
 36. D. Bertolini, T. Chan, and J. Thaler, *Jet observables without jet algorithms*, [Journal of High Energy Physics](#) **2014** (Apr., 2014).
 37. A. J. Larkoski, D. Neill, and J. Thaler, *Jet shapes with the broadening axis*, [Journal of High Energy Physics](#) **2014** (Apr., 2014).
 38. M. Cacciari, G. P. Salam, and G. Soyez, *FastJet User Manual*, [Eur. Phys. J. C](#) **72** (2012) 1896, [[arXiv:1111.6097](#)].
 39. J. Holguin, I. Moulton, A. Pathak, M. Procura, R. Schöfbeck, and D. Schwarz, *Top Quark Mass Extractions from Energy Correlators: A Feasibility Study*, [arXiv:2407.12900](#).
 40. S. Catani, Y. L. Dokshitzer, M. Olsson, G. Turnock, and B. R. Webber, *New clustering algorithm for multi-jet cross-sections in e^+e^- annihilation*, [Phys. Lett. B](#) **269** (1991) 432–438.